RYERSON UNIVERSITY
FACULTY OF ENGINEERING, ARCHITECTURE AND SCIENCE

DEPARTMENT OF AEROSPACE ENGINEERING

# Development of an automatic image cropping and feature extraction system for real-time warping monitoring in 3D printing

Jiarui Xie

AER870 Aerospace Engineering Thesis – Final Report

Faculty Advisor: Dr. Kazem Fayazbakhsh
Date: April 2020

## AUTHOR'S DECLARATION FOR ELECTRONIC SUBMISSION OF A PROJECT

I hereby declare that I am the sole author of this project. This is a true copy of the project, including any required final revisions.

I authorize Ryerson University to lend this project to other institutions or individuals for scholarly research.

I further authorize Ryerson University to reproduce this project by photocopying or by other means, in total or in part, at the request of other institutions or individuals for the purpose of scholarly research.

I understand that my project may be made electronically available to the public.

# DEVELOPMENT OF AN AUTOMATIC IMAGE CROPPING AND FEATURE EXTRACTION SYSTEM FOR REAL-TIME WARPING MONITORING IN 3D PRINTING

Jiarui Xie

## Abstract

Fused Filament Fabrication (FFF) is an additive manufacturing technology that can produce complicated structures in a simple-to-use and cost-effective manner. Although promising, the technology is prone to defects, e.g. warping, compromising the quality of the manufactured component. To avoid the adverse effects caused by warping, this thesis utilizes deep-learning algorithms to develop a warping detection system using Convolutional Neural Networks (CNN). To create such a system, a real-time data acquisition and analysis pipeline is laid out. The system is responsible for capturing a snapshot of the print layer-by-layer and simultaneously extracting the corners of the component. The extracted region-of-interest is then passed through a CNN outputting the probability of a corner being warped. If a warp is detected, a signal is sent to pause the print, thereby creating a closed-loop monitoring system. The underlying model is tested on a real-time manufacturing environment yielding a mean accuracy of 99.21%.

## Acknowledgement

First, I would like to express my sincere gratitude to my supervisor Dr. Kazem Fayazbakhsh from the Department of Aerospace Engineering at Ryerson University. He has been continuously and patiently supporting my thesis study with strong knowledge of Additive Manufacturing and clear insight of research potentials. The research experience and suggestions he shares with me have always been valuable, inspiring and encouraging.

I would also like to thank Dr. Zouheir Fawaz and students at FRAMES for the enjoyable experience I gain from such a fantastic and productive laboratory. Especially, I want to thank Mr. Aditya Saluja, who created the CNN warping classification model and makes my research possible.

Finally, I would like to thank my family and my girlfriend for their understanding, support and love.

# Contents

## Table of Figures

# Table of Tables

# 1. Introduction

## 1.1. Additive Manufacturing

The emergence and development of Additive Manufacturing (AM) technologies reveal more potentials of cost-effective and sustainable manufacturing [1]. Additive Manufacturing, also known as 3D Printing, constructs a 3D structure in a layer-by-layer methodology, directly guided by computer-aided design (CAD) data models [2]. Distinct from conventional subtractive manufacturing techniques, AM technologies can produce components with high structural complexity, as well as conserving a considerable amount of material [3]. When 3D Printing was first introduced into the industries, it was only considered as a fast way to create functional or aesthetical prototypes due to the limited material and poor strength. Therefore, it is called rapid prototyping at the beginning [4]. Nowadays, extensive research and enhancement on AM have improved the quality and efficiency of this manufacturing technology. On the one hand, more 3D Printing techniques are invented to allow more materials to be fabricated by AM. The materials now available for Additive Manufacturing methods include plastics, metals, ceramics, etc., adopted by various 3D Printing techniques such as Fused Filament Fabrication (FFF), Selective Laser Sintering (SLS), and Stereolithography (SLA) [5]. In addition, the 3D Printers are equipped with highly precise robotic systems and autonomous quality monitoring system. The possibility of a 3D printed part with low quality is significantly reduced. However, compared with other manufacturing technologies, such as molding and machining, AM cannot become a mass production method due to its slow speed and limited build volume [6]. It is also restricted by its limited printing material.

## 1.2. Fused Filament Fabrication

Fused Filament Fabrication (FFF) is also called Fused Deposition Modelling (FDM), which is the most widely utilized technology for both industrial and small-scale prototyping, as it can be highly user-friendly, automatic, and safe [7, 8]. Figure 1 depicts the typical layout of FFF 3D printers. The printing material of FFF 3D printers is usually long thermoplastic filament wound onto spools. Before the printing process starts, the CAD model of the part is sliced into layers by slicing software. In this process, an extruder continuously feeds filament into a heated nozzle and follows the printing paths defined by slicing software [9]. The thermoplastic filament is melted, deposited along the designated path, and cooled down to the solid-state. Once one layer is completed, the print bed or extruder will adjust its height and the next layer will be printed upon the previous ones [10, 11]. Additional support structures are needed if the upper layers cannot be directly supported by the lower layers.

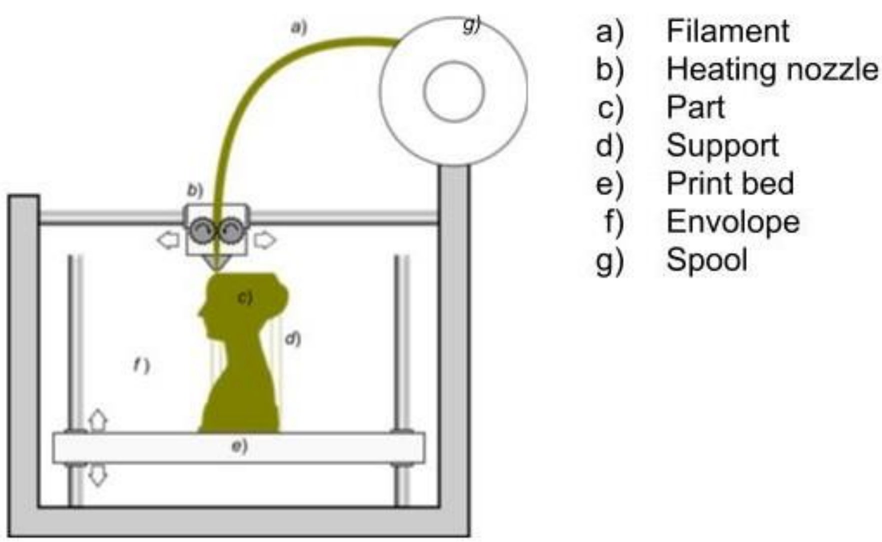


**Figure 1. FFF 3D printer. Source: Adopted from [12].**

According to the material and geometry of the part, the printing parameters need to be adjusted to improve the print quality with better adhesion, desired accuracy and less defect. The crucial parameters of an FFF 3D printer include layer thickness, extruder speed, infill ratio, extruder head temperature, print bed temperature, etc. [13].

## 1.3. Defects of FFF 3D Printing

Although FFF 3D printers offer an automated manufacturing technique to reduce time, cost, and material usage, defects are often observed from 3D printed objects, seriously compromising the printed products' quality and even damaging the 3D printer. The typical defects of FFF 3D printing are over/under extrusion, gaps, layer shifting, etc. [14]. In addition, warping can happen during 3D printing that can result in low dimensional accuracy, print failure, and even damage to the 3D printer.

## 1.4. Defect Monitoring and Diagnostics on FFF 3D Printing

To detect any defect exhibited by the part, mitigate the negative impact brought by them and improve the quality of 3D printed components, non-destructive testing (NDT) technologies are widely utilized in various in-situ defect monitoring systems. Non-destructive testing, also known as non-destructive inspection, examines the quality or property of a component, a structure or a system without decomposing or damaging the original tested object, using NDT techniques such as thermography, acoustic emission and vision-based analysis [15]. The applications of NDT on AM have been intensively researched and realized. However, there are several difficulties of NDT application on 3D Printing [16]:

- Characterization of defects: The quality monitoring system needs to be taught "what defects are". Since different industries and components have their own standards and tolerances, defects are hard to be universally defined by the system designers.
- Complexity of geometry: 3D printing allows the users to print complicated geometries, including internal geometries that are usually difficult to access by the NDT technologies.
- AM materials: Different FFF 3D Printing materials, i.e. polymer and composite, have different types of defects.

- AM processes: Some 3D printers' hardware setup does not readily allow the NDT equipment to be installed. The others, however, might not provide open source software that promises the data transmission and closed-loop control.

A literature review section will introduce the rationales and equipment layout of different FFF 3D Printing quality monitoring system. Their experience and methodologies will be studied to inspire and improve the monitoring system to be designed.

## 2. Literature Review

The literature review was performed with respect to the research effort of warping mitigation and NDT systems applied to FFF 3D printers. It is important to understand how warping happens (Figure 2). After material deposition, since the cooling rate is not uniform throughout the print, the temperature gradient in the part creates residual thermal stress [17, 18]. As the number of deposited layers increases, the residual thermal stress builds up in the part and might distort it when the adhesion between the part and the heat bed (HB) is not enough to overcome the bending force. Warping usually starts from the corners and results in the part being peeled away from the print bed [19].

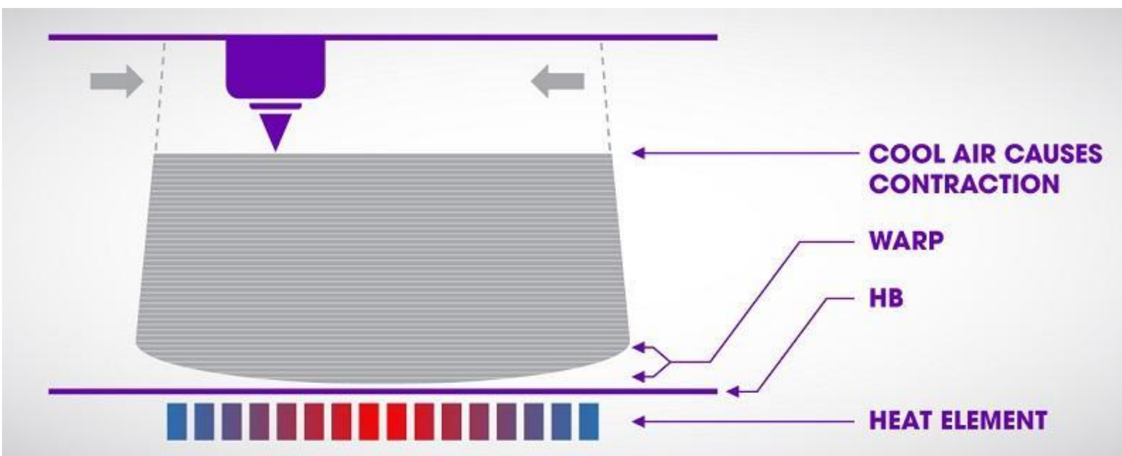


**Figure 2. The formation of warping [20].**

## 2.1. Mitigation of Warping

Warp deformation can be primarily ascribed to material properties, process parameters, and part geometry. Several studies have been performed on the analysis and optimization of factors that lead to warping. Wang et al. [18] developed a mathematical model and identified number of layers, chamber temperature, and material thermal expansion rate as significant parameters which may lead to warp deformation. Fitzharris et al. [21] investigated the impact of material properties on warpage by altering material parameters of polyphenylene sulfide (PPS) gradually to polyphenylene (PP). It was observed that a low thermal expansion rate and high thermal conductivity would help prevent warping. Peng et al. [22] also indicated that filament treatment to decrease its glass transition temperature and thermal expansion coefficient before 3D printing could lower the chance of warping. In a study conducted by Alsoufi et al. [23], process variables were monitored to find an ideal nozzle temperature and printing speed for advanced polylactic acid (PLA+). Similarly, Panda et al. [8] studied the impact of four process parameters and concluded that layer thickness and printing speed are more important than filling speed and line width compression regarding warping prevention. Singh [24] investigated the chemical treatment of the build platform, enclosure, and internal structure of the model to overcome warp deformation. Armillotta et al. [25] conducted experiments on the influence of part geometric parameters on warping. They demonstrated that as the maximum dimension of the part horizontal plane decreases there is a lower chance of warping. Based on this finding, Guerrero-de-Mier et al. [26] developed bricking technique, whereby layers were divided into squared or hexagonal sections to reduce the maximum dimension of the part horizontal plane and the chance of warp deformation.

## 2.2. Non-Destructive Testing on FFF 3D Printing

The above studies explored, analyzed, and optimized parameters that impact warping. Alternatively, many researchers have been putting their effort on NDT systems to monitor many types of defects, reduce the waste of material, avoid damage to the printer, and enhance the quality of the print.

### 2.2.1. Thermography

Thermography measures the temperature distribution of the surface of an object using thermal cameras. It essentially captures and measures the electromagnetic radio spectrum, especially the infrared band, emitted from the heated object. The intensity of the spectrum at different wavelengths reflects the temperature of the surface [16]. To obtain an accurate temperature distribution, the system needs to be calibrated according to the emissivity of the object, the surrounding and the atmosphere. The essence of quality monitoring system utilizing thermography is that any surface flaw would change the local heat transmission so that the cooling rate is different at the flow area and other parts of the surface. Thus, such a surface defect including cracks, voids, delamination and layer shifting could be recognized by thermal imaging. There are two types of thermography: passive and active thermography. With respect to FFF 3D Printing, passive thermography detects the heat flow of the natural cooling of the print, as the material is heated to semi-solid state and then cooled naturally. Active thermography introduces an external heat source to heat up the surface of the object. With the external heat source, the heat will propagate through the subsurface and detect any defect inside. Figure 3 demonstrates the hardware layout of an active thermographic monitoring system applied to FFF 3D printers. A control unit is connected to a computer to coordinate the external heat source and the infrared camera. The excitation source heats up the specimen and the infrared camera captures and sends the image to the control unit and then the computer. The computer generates and analyzes the thermal field of the specimen based on the thermal distribution to reveal the defects within the subsurface of the object. The effective range of defect detection for thermography is usually 0 to 10 mm under the surface [27].

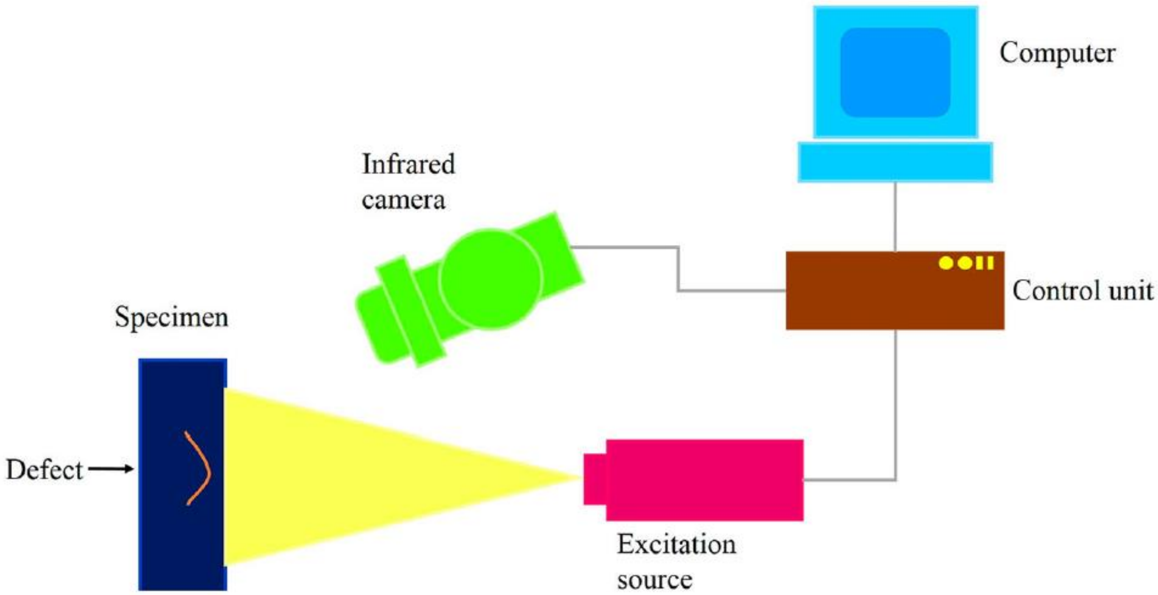


**Figure 3. Hardware setup of an active thermography monitoring system on 3D printers [16].**

Lu and Wang [28] have made some improvements on thermographic defect monitoring on AM using physics-based compressive sensing (PBCS). PBCS allows the computer to reconstruct the thermal imaging with high-fidelity using low-end thermal cameras that can only provide limited information. Therefore, the quality monitoring system can detect defects with low-budget equipment and a smaller number of thermal cameras.

The advantage of the monitoring techniques based on thermography is that they do not require any contact between the measurement tool and the part. However, the difficulty to implement such a system is high because the temperature field of the part is also affected by the surroundings. It is hard to calibrate the camera to get an accurate temperature distribution measurement considering the changing materials, geometries and environments. Different materials and geometries will lead to different heat transfer rate so that the system needs to be trained accordingly. Also, the environmental conditions such as the distance between the camera and the part or object being heated by other heat sources nearby make the system hard to be applied to FFF 3D Printing. Additionally, this method is restricted to detecting the defects only on the surface and subsurface of the print.

### 2.2.2. Vibration Sensor

Li et al. [29] developed an in-situ FFF 3D Printing monitoring system that monitors both the state of the printer and the quality of the print with vibration sensors. As Figure 4 indicates, four vibration sensors are attached to the FFF 3D printer: one is attached to the build platform, the other three are attached to the extruder. When the FFF 3D printer is working, the vibration will be received by the sensors, transformed to electrical signals and sent to the computer for data processing and analysis. The researchers managed to find the special modes of the vibration that could represent filament jam, warpage and extruder leakage. For example, when the corner of the print is warped, the vibration strength of the print bed and the extruder will be reduced. Then, some features from the reduced vibration signals denoting warpage could be extracted.

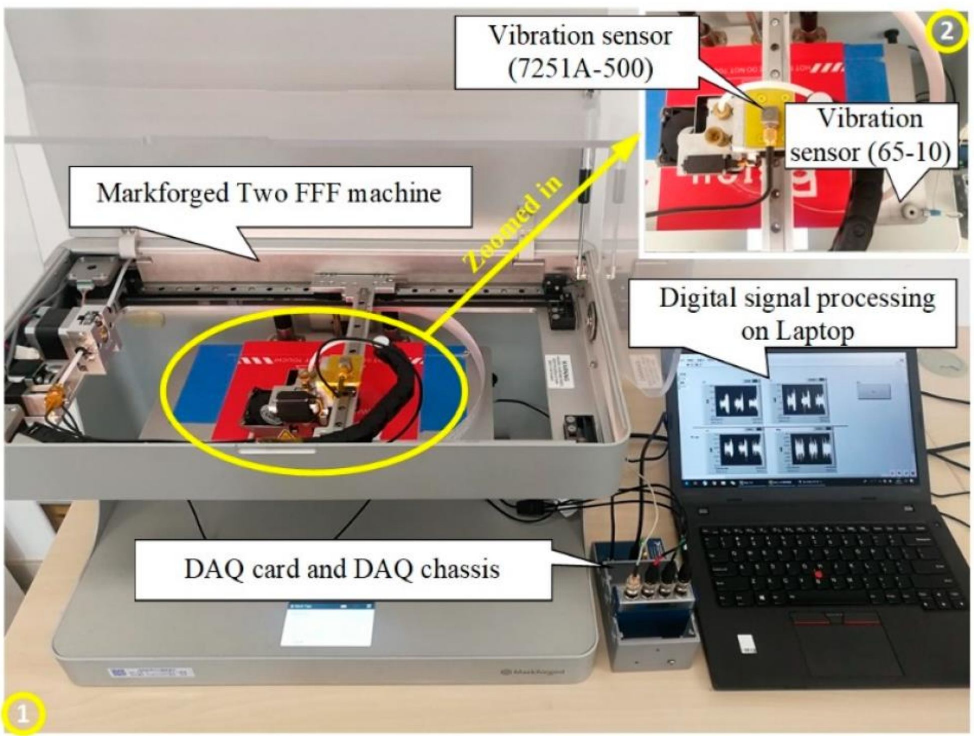


**Figure 4. FFF 3D printer's monitoring system using vibration sensors [29].**

The merit of vibration sensors being adopted is that multiple machine state errors exist. However, it is hard to characterize the defects and state errors based on vibration as different machines and geometries would likely change the vibration features representing different defects. Further, this method requires multiple vibration sensors to be attached to the printer and build platform, which might not be allowed by the hardware setup.

### 2.2.3. Acoustic Emission Testing

Acoustic emission is the acoustic wave in a solid object as an irreversible process developing. It could be produced by a sudden release of energy such as fracture and cracking. I can also be a gradual release of stress such as plastic deformation. Thus, Wu et al. [30] proposed and designed a quality monitoring system for FFF 3D printers using acoustic emission testing. Such a system has been proven effective in the detection of filament jam, warpage, filament run-out and filament breakage [30, 31]. The general processes are indicated in Figure 5. A transducer, which senses acoustic wave pulses and transfers them into electrical signals, is attached to the part. The signals are first sent to a pre-amplifier and then pass through a filter to reduce the noises. Afterwards, the signals are amplified again and processed to extract the important features.

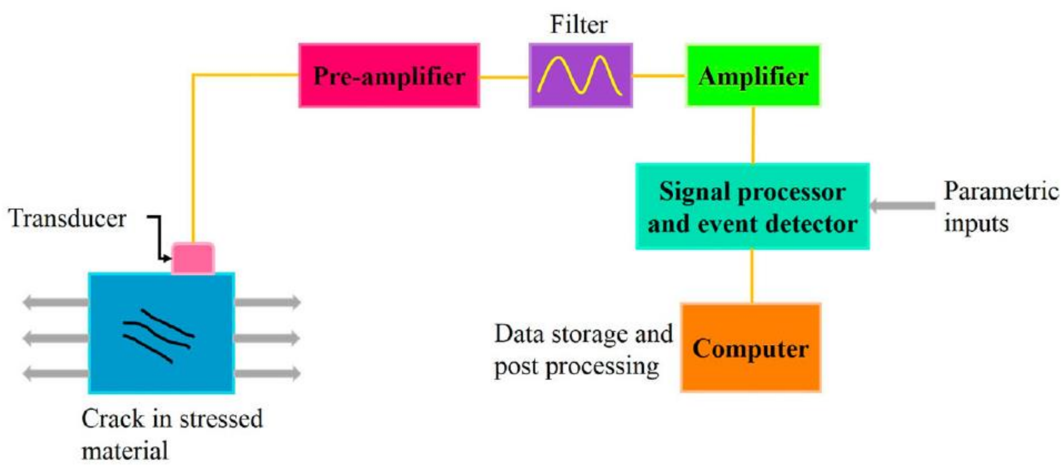


**Figure 5. General layout and procedures of a quality monitoring system based on acoustic emission testing [16].**

It was discovered that from the acoustic waves received by the transducer, several types of the defect or machine state errors can be detected and differentiated. Nonetheless, this method is not contactless, meaning the transducer needs to be attached to the part. For FFF 3D printing, this requires that the print must be stopped to attach the transducer and the geometry readily provides the space for the transducer. Again, depending on the machine and geometry, the defects and state error need to be characterized accordingly.

### 2.2.4. Fiber Bragg Grating Sensing Technology

Fiber Bragg Grating (FBG) sensors are embedded in a straight optical fiber. Depending on the strain of the optical fiber, certain wavelengths will be reflected by the FBG sensors as light passing through. Therefore, the strain of a component can be measured using FBG sensors. Fang et al. [32] deployed an FBG sensor on an FFF 3D-printed part to monitor its strain shown in Figure 6. They found that the FBG sensors are eligible to measure the deformation and help inspect the integrity of the 3D-printed components. Kousiatza and Karalekas [33] used both FBG sensors to measure the strain of the print and a thermocouple to measure the temperature profile of the part being printed by an FFF 3D print on an in-situ basis (Figure 7). They discovered that the residual stress built up during the printing process could be measured by FBG sensors.

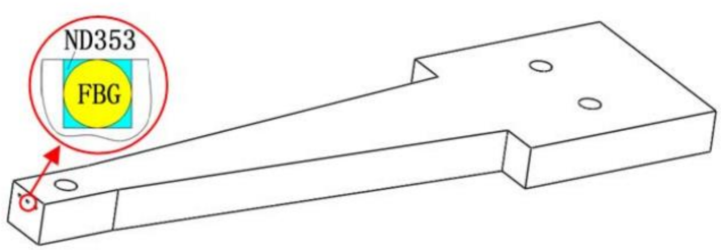


**Figure 6. FBG sensors deployed on a 3D-printer component [32].**

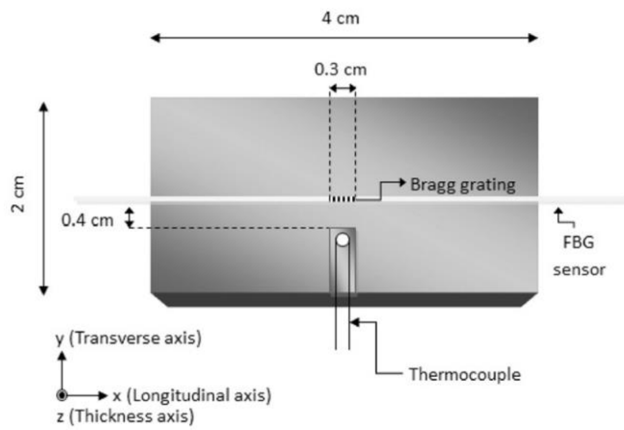


**Figure 7. FBG sensor and thermocouple deployed on a 3D -printed part to measure the strain level and temperature profile [33].**

FBG sensors accurately reflect the strain level, but it does require good straightness of the surface. Considering the residual stress being built up through the print, the part is likely to be distorted, affecting the quality of FBG measurement. Also, the 3D-printed part might not be readily available for the installation of the FBG sensors.

### 2.2.5. Vision-based Defect Detection System

Straub [34] proposed an initial design of an FFF 3D Printing progress monitoring system with low-budget Raspberry Pi cameras deployed around the 3D printer shown in Figure 8. During the print, the cameras will take pictures periodically and send the images to the computer via USB connection. According to Straub's tests, as the part building up, the brightness of the image was reducing. Thus, the completeness of the print job can be monitored.

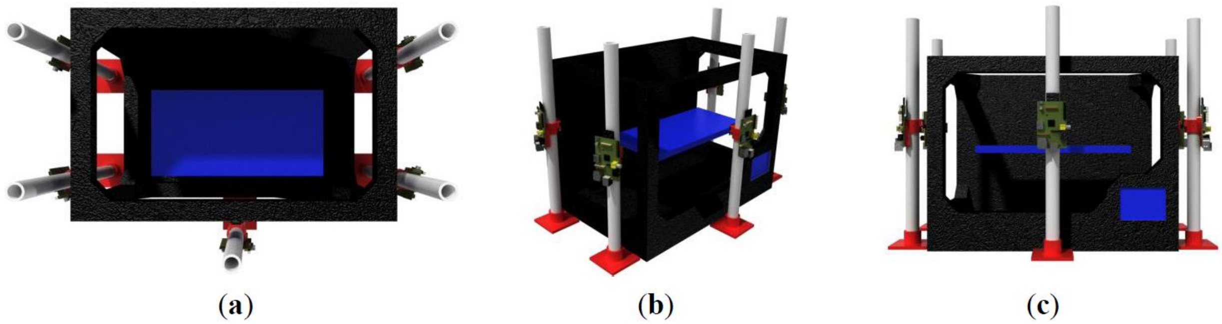

**Figure 8. Vision-based progress monitoring system with microcomputers: (a) top view; (b) oblique view; and (c) front view [34].**

Baumann and Roller [35] devised a single-camera system that was able to inspect printing errors such as warpage and over/under extrusion with accuracy between 60% and 80%. They attached 6 optical markers to the 3D printer and cropped the area enclosed by them (Figure 8 (a) and (b)), which merely helped to reduce the noises from the background and saved computational power. Also, they tried to extract the part's contour based on the HSV (Hue-Saturation-Value) color model (Figure 8 (c)), but the result cannot support defect detections with high accuracy.

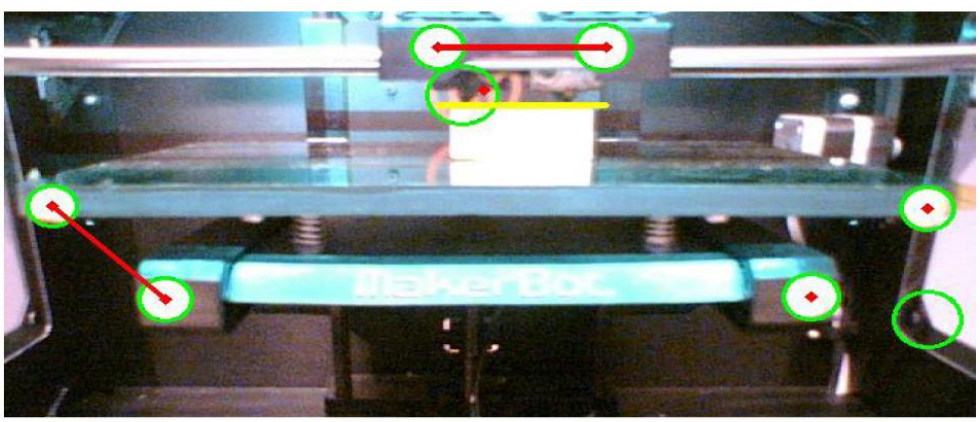

**(a)**

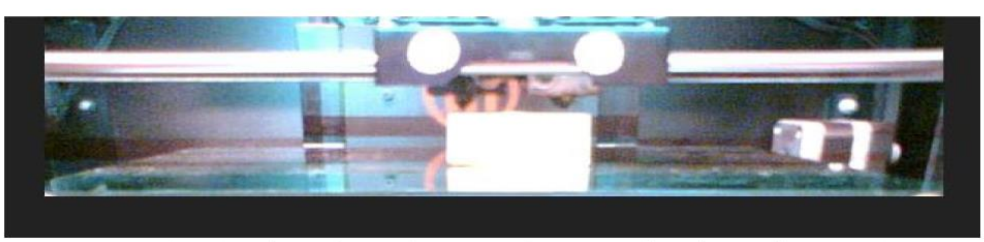

(b)

(c)

**Figure 9. Image cropping of the vision-based 3D printing quality monitoring system with optical markers: (a) original picture; (b) cropped image; and (c) part's contour extracted [35].**

Holzmond and Li [36] utilized a three-dimensional digital image correlation (3D-DIC) system that incorporated two cameras to take images and constructed a data model of the print. As Figure 10 demonstrates, two cameras were mounted on the top of the 3D printer, capturing the image of the part at different angles to virtually construct a point cloud model of it. Two lamps were installed at the top and right side of the printer to provide greater brightness required by the 3D-DIC system. The data model was then compared with a point cloud containing the information of the design model extracted from its G-code to check for anomalies in the printed part. This work did not provide sufficient test data to demonstrate the reliability of the 3D-DIC system or its accuracy. Furthermore, this technique involved intensive data transformation and simulation, which required high computational power and lowered the speed of defect detection.

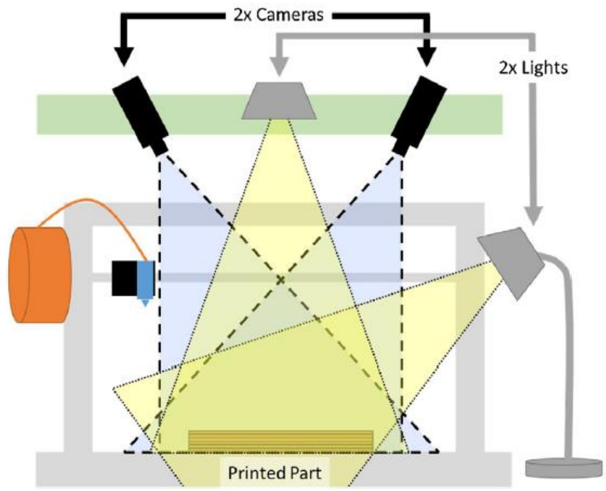


**Figure 10. 3D-DIC quality monitoring system on FFF 3D Printing [36].**

Liu et al. [37] designed a closed-loop quality control system for FFF 3D Printing using textural analysis-based image diagnosis (TA-ID) algorithm. As Figure 11 indicates, two digital microscopes were deployed at the two sides of the extruder to capture clear close-up images of the part's texture. Then, the images were cropped manually to keep a small region of texture for image analysis. The images were processed and features relative to the filament flow rate were extracted. They built a closed-loop control system with a PID controller that adjusted the flow rate according to the images captured in-situ. Thus, the quality of the print can be improved on a real-time basis.

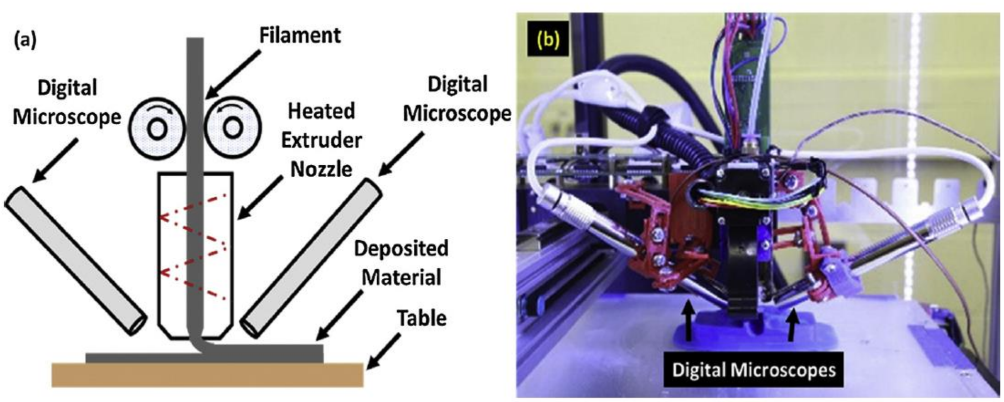


**Figure 11. Hardware setup of the closed-loop TA-ID quality monitoring system for 3D-printed part: (a) 2-D sketch; and (b) Actual equipment [37].**

### 2.2.6. Objective

The above literature review reveals what kind of NDT technologies have been incorporated into in-situ FFF 3D Printing quality monitoring systems along with the rationales and equipment setups. The advantages and disadvantages of different methods were illustrated. Vision-based monitoring systems possess lots of merits over other techniques:

- It is contactless and the deployment of the cameras are flexible.
- Images can provide comprehensive information for feature extraction.
- Many algorithms such as computer vision and machine learning can be utilized.
- Features would not change so much as acoustic emission and vibration signals do.

The review of the previous vision-based systems also indicated that none of the vision-based autonomous in-process defect detection systems applied on FFF AM has been developed with efficient automatic image cropping functionality. The benefits of an automatic image cropping system are of higher accuracy and faster analysis. When the irrelevant features in the image are eliminated, the classification model receives an input that is highly similar to its training images, leading to accuracy as high as the original model under ideal conditions. Further, cropped images have fewer pixels, which reduces the time needed for image analysis. Automatic feature extraction also reduces human intervention so that the system is not affected by human error and decreases the labor cost. Therefore, this refined in-process warping monitoring system incorporates an automatic feature extraction system that locates and crops the region of the image where the corner of the part exists during the printing operation.

This thesis report will introduce an autonomous closed-loop warping monitoring system with automatic feature extraction system including image cropping and Convolution layers. The hardware layout, software setting, and real-time analysis procedures will be demonstrated and explained. The essential algorithm of convolutional neural network (CNN) classification model that differentiates the warped corner from unwarped corners was created by my colleague, Aditya Saluja. This project works on the implementation of a practical closed-loop monitoring system that would terminate the print once a warped corner is detected. When a layer of the print is finished, the printer will stop for 4 seconds and the camera will automatically capture an image of the corner to analyze. The major difficulty of such a system is the location of the warping, given that the print bed keeps moving. The part's corner, where warping usually starts from, is cropped from the image using a novel feature extraction proposed by this research. The corner is located on the image with G-code analysis and correlation method based on map-matching. The review of current research achievements on defect detection of FFF 3D Printing is first revealed. Then, the methodology and procedures of the proposed system are illustrated. Finally, the test plan and results are shown to validate this design.

# 3. Methodology

## 3.1. Hardware Setup

Figure 12 demonstrates the hardware setup of the warping monitoring system. A Prusa i3 MK2S FFF 3D printer is selected as our experimental printer because it typically represents a wide range of FFF 3D printers that have a print bed moving in Y direction and an extruder moving in X and Z directions. A hardware system that works for this printer can be applied to many other FFF 3D printers. Also, it can be communicating with computers through USB connection so that a closed-loop control can be designed and deployed with a Raspberry Pi. In our experiment, the training and testing images were captured from the sample coupons printed with white and grey PLA filaments. To mitigate the effect of reflection, blue or green non-reflective painter's tape were used.

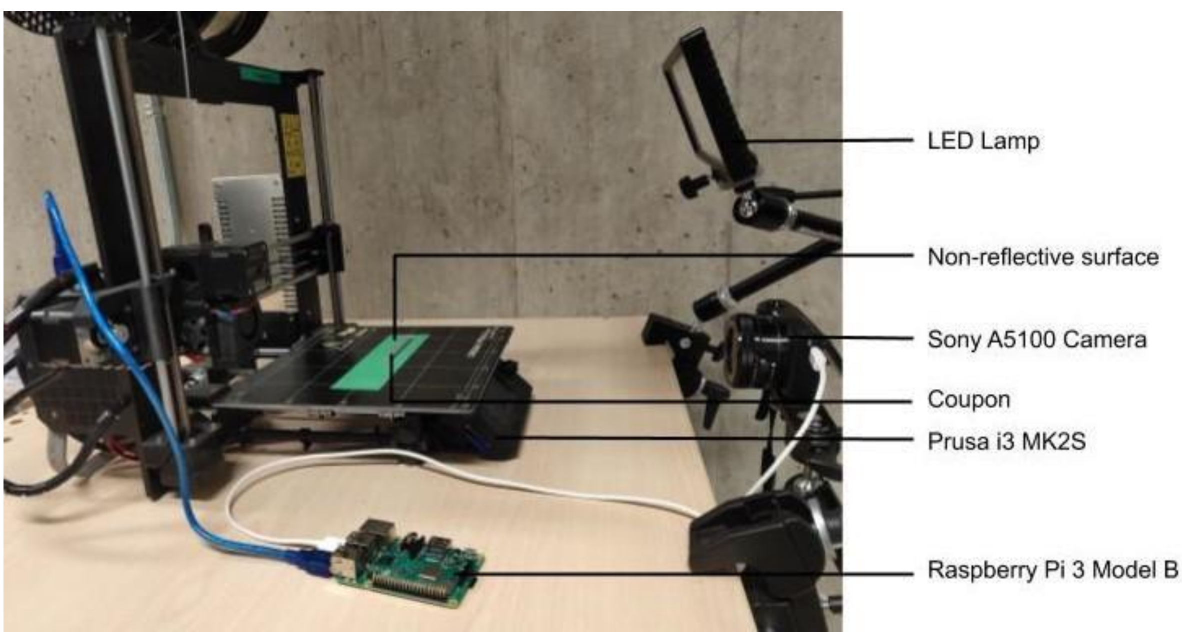


**Figure 12. The experimental layout of the closed-loop in-process warping monitoring system.**

A Sony A5100 camera is placed in front of the 3D printer and at the same height as the print bed, capturing the image of the side view of a part. As shown in Figure 13, the blue region indicates the area covered when the print bed moves from the most forward to the most backward location in Y-axis. The orange zone is the region of interest (ROI) that the left corner of the part will exist during the tests. The real-time image analysis will primarily be performed on the left corners of the print in the experiments. The camera will be placed at orientation A (orthogonal to X-axis) and B (75 degrees at X-axis) respectively to test the system. To capture clear images of the corners within the ROI, the F-number of the camera needs to be increased to obtain the largest depth of field so that the camera can remain focus over a wide area on the print bed. However, the brightness will be reduced due to less light passing through the lens. Thus, an LED lamp is deployed right above the camera to increase the light intensity. The F-number and LED lamp's angle were carefully adjusted so that clear images of the corners within the ROI can be captured with no significant flare. The optimal F-number and the lamp's angle are F18 and 70 degrees.

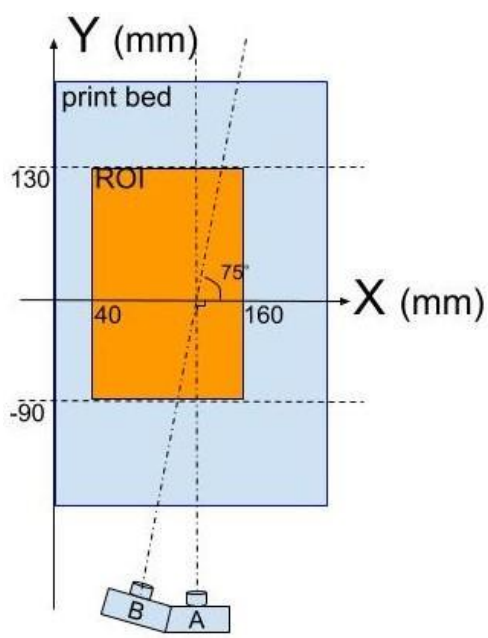


**Figure 13. Print bed coordinate system: Region of interest regarding the left corner's location**

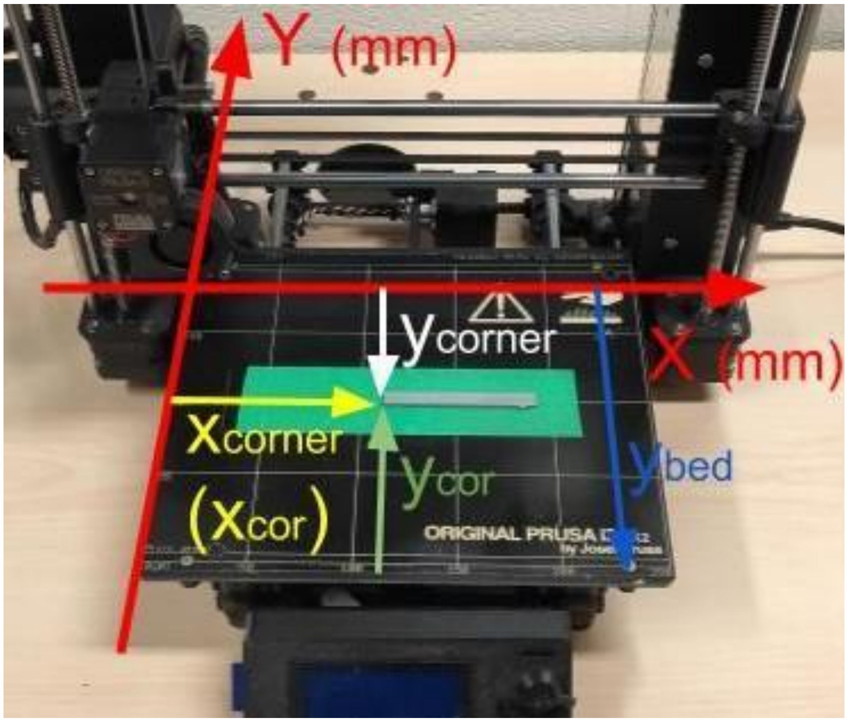


**Figure 14. Definition of corner's position in the print bed coordinate system.**

A Raspberry Pi 3 Model B pre-configured with OctoPi is connected to the printer and the camera by two USB cables. It has a Quad-Core ARMv8 processor with 1GB RAM running on Linux, which has sufficient computational power for the classification model, G-code analysis and feature extraction.

## 3.2. Software Setup

OctoPrint is an open-source web server and interface for 3D printing written in Python. It allows the users to download and create plugins so that they can add more functionalities and customize the printing operations. Figure 15 depicts the general procedures of the information transferring between the components, forming a closed-loop system. The computer first uploads a G-code script to the OctoPrint server. Then, the Raspberry Pi downloads the G-code via wireless connection and analyzes it with the OctoPrint plugins. Briefly speaking, the plugins of the system automatically find the layer changes, retrieves the real-time position of the corner from the G-code and pauses the print for 4 seconds. Controlled by the plugins, the camera will capture an image when the printer pauses and store it into the Raspberry Pi. To acquire an accurate result, the image needs to be cropped so that only the corner remains as the classification model is trained with pictures that only contain the corner.

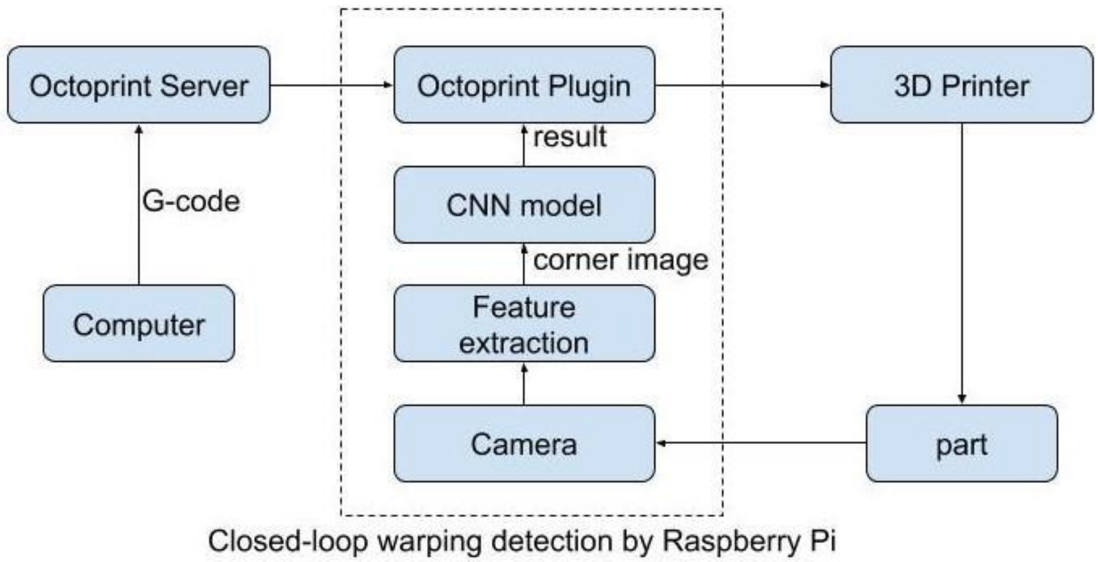


**Figure 15. Flow chart of the closed-loop warping detection procedures.**

Figure 16 shows the desired region to be cropped and inputted into the classification model. The corner to be analyzed is indicated in the red box, and the cropped image is generated by the feature extraction system. Figure 5 also defines the coordinate system of the image captured. The feature extraction tool is a correlation system that correlates the corner's position in the image coordinate system ($x'_{image}$) with its position in the print bed coordinate system ($x_{corner}$ and $y_{corner}$). It is assumed that when the camera is placed at the same height as the print bed, the vertical position of the corner on the image ($y'_{image}$) will not vary significantly; and thus, can be considered as a constant number. After the cropped image is acquired, it will be inputted into the CNN classification model. Based on the classification model's result, the OctoPrint plugin will choose to continue or terminate the print. Hence, a closed-loop system is formed.

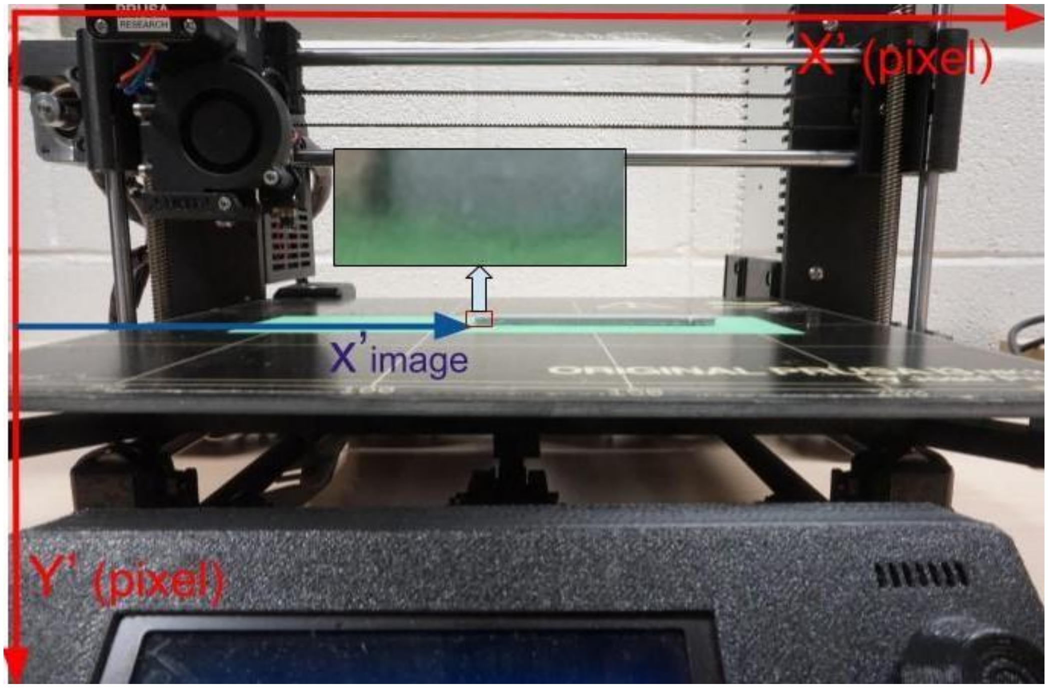


**Figure 16. Image captured by the camera and the desired region to be cropped.**

### 3.2.1. Image-Print Bed Coordinates Correlation

The benefits of an automatic feature extraction system are higher accuracy and faster analysis. When the irrelevant features in the image are eliminated, the classification model receives an input that is highly similar to its training images, leading to accuracy as high as the original model under ideal conditions. Further, cropped images have fewer pixels, which reduces the time needed for image analysis. Automatic feature extraction also reduces human intervention so that the system is not affected by human error and decreases the labor cost. Therefore, this refined in-process warping monitoring system incorporates an automatic feature extraction system that locates and crops the region of the image where the corner of the part exists during the printing operation.

By analyzing the G-code commands, the location of the corner in the print bed coordinate system can be obtained. To crop the image, the location of the corner in the image coordinate system is required. The purpose of the correlation is to estimate the location of the corner on the image using its location on the print bed. Therefore, a map-matching between the two coordinate systems is performed.

### 3.2.1.1. Automatic Data Collection

112 reference points within the ROI shown in Figure 17 (a) were created. The reference points are equally spaced except three rows inserted at $y_{corner}$=0, $y_{corner}$=120 and $x_{corner}$=50. These three lines of reference points will not be used to train the interpolation model, but will be treated as testing data to validate the correlation. Two 3D printed parts were created to aid in automatic map matching (Figure 18). The upper part with a rectangular notch is mounted on the extruder block. The lower part is mobile and placed on the print bed. It has a rectangular block on the top that can slide into the upper part and a triangular platform pointing at the extruder's direction. The corner of the triangular platform is right beneath the extruder head, where a red marker is attached, representing the location of the reference point. The triangular platform has a lower height than the block to leave enough clearance between the extruder head and the part. When the lower part's rectangular block slides into the upper part's notch, the lower part can move with the extruder. And when they are detached, the lower part can move with the print bed. Hence, a G-code is prepared to automatically guide the lower part to each reference point. An OctoPrint plugin autonomously captures an image when the lower block arrives each point. The two parts will be taken off from the 3D printer after the data collection process.

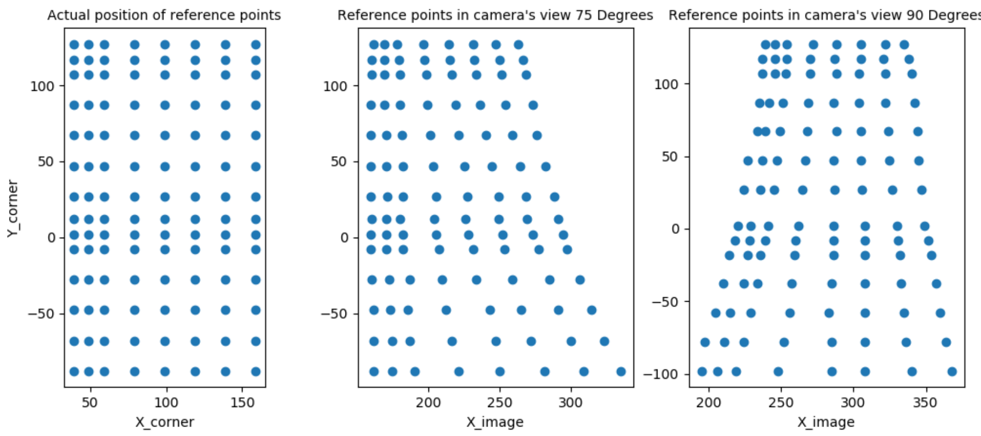


**(a)** **(b)** **(c)**

**Figure 17. Comparison between actual positions of the reference points and the distorted positions on the camera (75˚ and 90˚).**

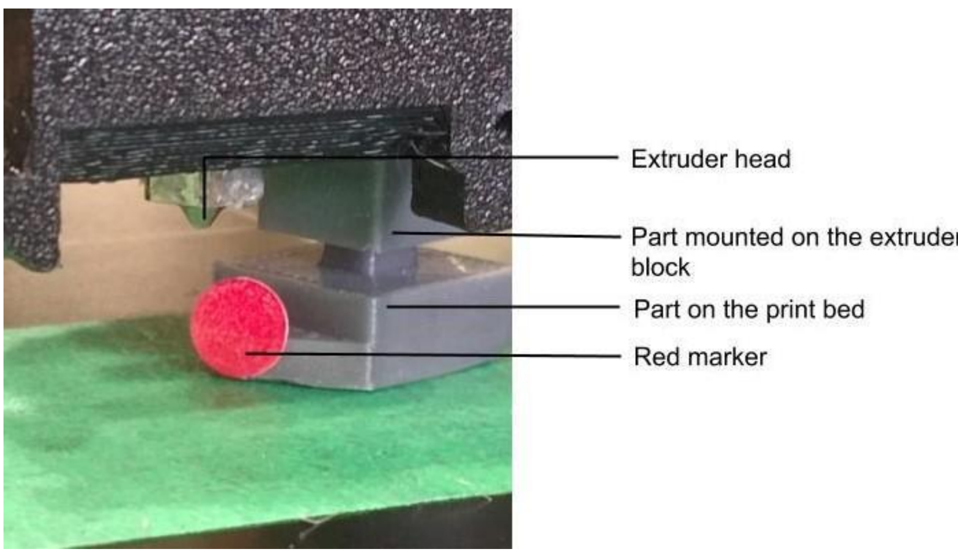


**Figure 18. Tools aiding in automatic correlation.**

Color recognition technology is used to find the location of the red marker. The Red-Green-Blue (RGB) color model is utilized to define the threshold of "red color" (Table 1). The original image captured, Figure 19 (a), will be put on a color mask so that only the pixels with an RGB color scale between the upper and lower bounds will be kept. In Figure 19 (b), the long red stripe at the top is the red wire and the red dot at the bottom is the marker. Then the red pixel at the very bottom will represent the corner's position on the image. And $x'_{image}$ is defined by the horizontal location of that pixel. In this way, the dataset to establish the correlation between the two systems can be collected for the 112 reference points. Each reference point's $x'_{image}$ value is corresponded to a pair of $x_{corner}$ and $y_{corner}$. The position of any point within the ROI can be determined using interpolation.

**Table 1. Red color threshold's upper and lower bounds.**

| | R | G | B |
|---|---|---|---|
| Lower bound | 17 | 15 | 100 |
| Upper bound | 50 | 56 | 200 |

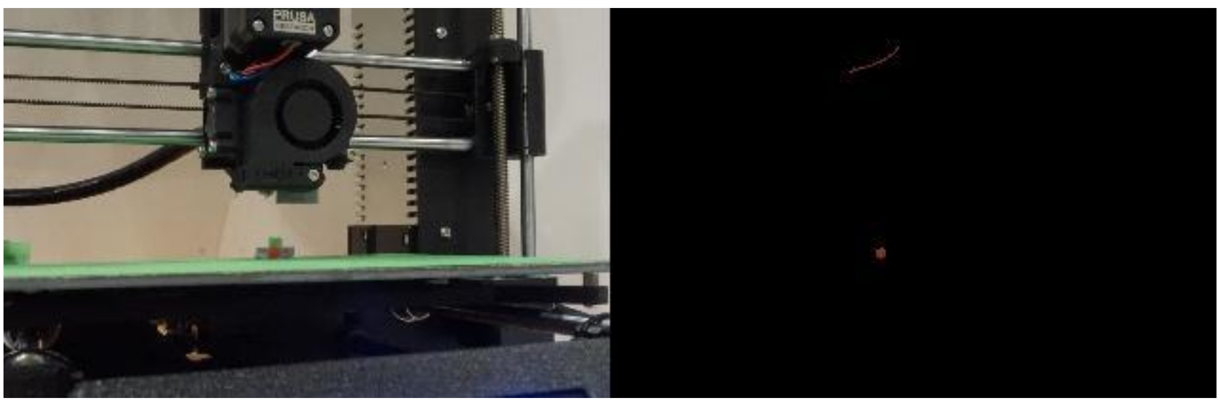

**(a)** **(b)**

**Figure 19. A red marker used to define the reference point's position on the image (a) original image; and (b) image with red color mask.**

Considering the practical production or laboratory environment, the technician might not place the camera precisely perpendicular to the X-axis and right at the centerline of the print bed. The correlation system is designed in such a way that it can accurately locate the corner even the camera has angles or displacement from the centerline of the print bed. In this experiment, the camera was placed perpendicular to the X-axis and then at 75 degrees facing at the center of the print area. Figure 17 (b) and (c) are the $y_{corner}$ vs $x'_{image}$ plots of those reference points, which indicate that the images are distorted in the camera's view. Depending on the lens, radial distortion will occur and make the image skewed. Thus, linear interpolation should not be selected as the relationship is not linear. Instead, spline interpolation is chosen.

### 3.2.1.2. Bivariate Spline Interpolation

Spline interpolation is a numerical approximation method that uses a piece-wise polynomial named spline. Taking three points $A(x_{i-1}, y_{i-1})$, $B(x_i, y_i)$ and $C(x_{i+1}, y_{i+1})$, where $x_{i-1} < x_i < x_{i+1}$, two polynomial curves $L_1$ and $L_2$ were created to smoothly connect them. Point B is the intercept of $L_1$ and $L_2$.

$$L_1(x_{i-1}) = y_{i-1} \tag{1}$$

$$L_1(x_i) = y_i \tag{2}$$

$$L_2(x_i) = y_i \tag{3}$$

$$L_1(x_{i+1}) = y_{i+1} \tag{4}$$

Cubic spline is the classical approach. A cubic spline should be smooth at the joint so that the two curves have the same slope and concavity at point B:

$$L_1'(x_i) = L_2'(x_i) \tag{5}$$

$$L_1''(x_i) = L_2''(x_i) \tag{6}$$

To solve for the equation of the two curves, it is required to assume the boundary conditions. Natural spline boundary conditions are commonly adopted to generate a natural and smooth interpolation, where the second derivative of the two ends A and B are equal to zero:

$$L_1''(x_{i-1}) = 0 \tag{7}$$

$$L_2''(x_{i+1}) = 0 \tag{8}$$

Thus, two polynomial curves can be acquired to form a univariate spline. In this correlation, there are two input variables, $x_{corner}$ and $y_{corner}$. To solve for an interpolation result with two variables, smoothing bivariate spline approximation tool from SciPy is introduced to the correlation procedure. SciPy is an open-source software tool written in python, aiding in the solution of various mathematical problems. Additionally, the degree of the bivariate smoothing spline was set to 3 (cubic spline for both variables) in the experiments.

To validate the interpolation result, the actual $x'_{image}$ positions from the testing dataset will be compared with the interpolated results. Root mean squared error (RMSE) is used in the validation. A small RMSE value indicates a good interpolation model.

$$RMSE = \sqrt{\frac{1}{n}\sum_{j=1}^{n}(x_{image,j} - \hat{x}_{image,j})^2} \tag{9}$$

where n (n=28) is the number of the testing reference points, $x_{image}$ is the dataset of the interpolation results, and $\hat{x}_{image}$ is the testing dataset.

### 3.2.2. OctoPrint Plugin

OctoPrint plugins are the skeleton of the system. They are responsible for multiple tasks such as G-code analysis, G-code editing, picture transfer, etc. This section will introduce the roles the plugins play to reveal the workflow of the warping monitoring system in detail. Figure 20 is the block diagram that demonstrates the algorithm. The G-code of the part will be downloaded to the Raspberry Pi 3 once the user activates the print job on the OctoPrint website. The G-code will first be queued in the Raspberry Pi before it is sent to the printer. The 3D printer will receive five G-code commands from the Raspberry Pi at each turn and request another five commands when the previous commands are being executed. As the G-code commands are in the queue, the OctoPrint plugins can still edit them.

The plugins will scan through the queue and look for commands with “Z”, indicating layer changes. For the first a few layers, the printer will not be paused, but analyze the G-code to find the left corner of the print on the print bed ($x_{cor}$ and $y_{cor}$ shown in Figure 2 (b)). The logic is indicated below:

- Parse the G-code command if in this form “G0/G1 X(number) Y(number)”
- Store the numbers following “X” and “Y” into arrays $x_{coordinate}$ and $y_{coordinate}$, respectively.

- Take the minimum in array $x_{coordinate}$ as $x_{cor}$ and pull out the corresponding numbers from $y_{coordinate}$
- Take the minimum of the elements chosen from $y_{coordinate}$ from the last step as $y_{cor}$

This way, the system can detect the corner's coordinate of multiple geometries such as rectangular, rounded and triangular corners. Once a layer change is detected, the plugin will insert a pause command (G4) to pause the print before the layer change. While the printer is paused, the location of the print bed $y_{bed}$ will be retrieved from the G-code. The input to the correlation can be obtained:

$$x_{corner} = x_{cor}$$

$$y_{corner} = y_{cor} - y_{bed}$$

Then, the plugins will send a command to the camera so that an image is captured when the printer pauses. Based on $x_{corner}$ and $y_{corner}$, the correlation model provides $x'_{image}$, allowing the algorithm to locate and crop the image. The cropped image only contains the important features, which is the corner in our system. Afterwards, the cropped image will be sent to the CNN classification model for image analysis. The output result is a probability that the corner is not warped. A threshold of 0.3 is chosen, meaning that if the result is less than 0.3, the corner is considered a warped corner. The threshold is set to 0.3 instead of 0.5 because after analyzing the classification results of the training and validating dataset, a warped corner usually has a result of less than 0.01. Thus, the threshold is adjusted to a smaller value from 0.5. Depending on the classification result, the Raspberry Pi will continue or abort the print.

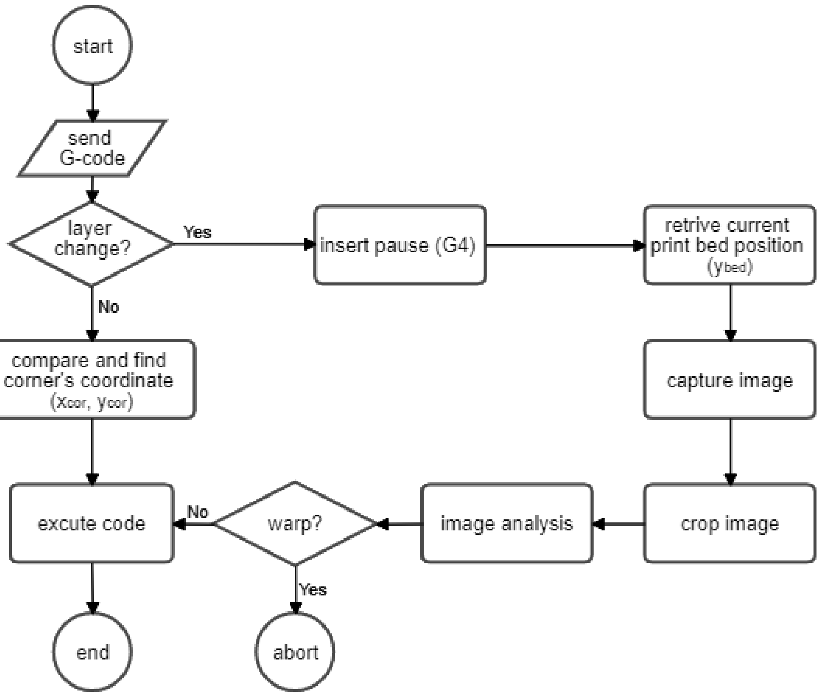


**Figure 20. Block diagram of the system.**

## 4. Result and Discussion

This section presents the test results of the refined closed-loop in-process warping monitoring system, including hyperparameter optimization, image-print bed correlation and real-time warping detection on sample coupons.

### 4.1. Correlation Results

Figure 21 demonstrates the surface generated from the correlation results based on bivariate spline interpolation in comparison with the original reference points' scatter plots. Root mean squared error is used to initially evaluate the interpolation results. The RMSEs were 0.84 at 90-degree and 0.64 at 75-degree, respectively. The small RMSE values revealed that the difference between the actual values and the correlation results of the testing points were minimal.

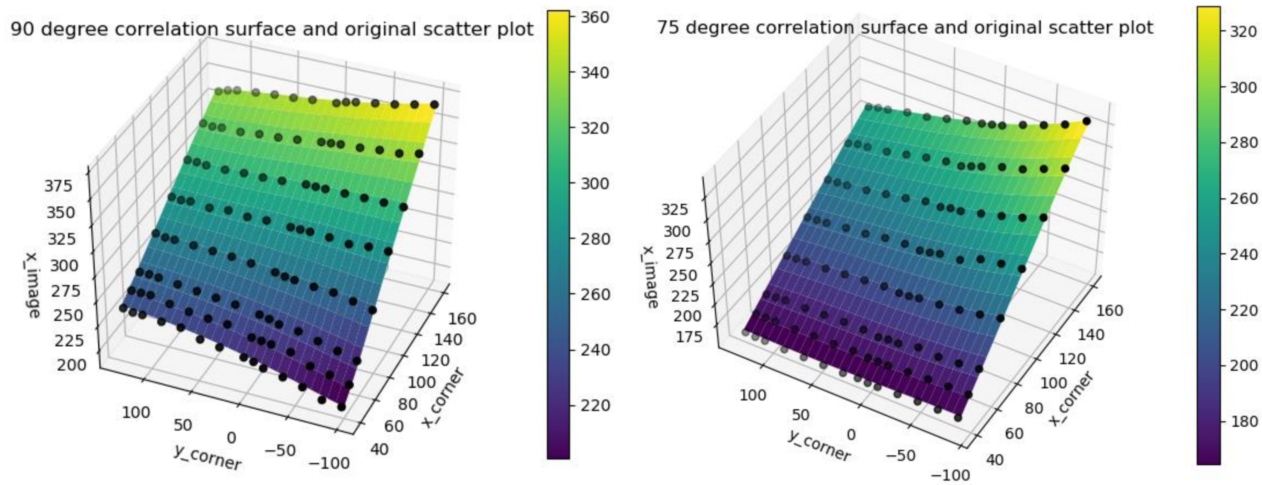


**(a)** **(b)**

**Figure 21. Correlation surfaces and original reference points' scatter plots (a) 90 degrees; and (b) 75 degrees.**

## 4.2. Warping Monitoring System

To further validate the system, warping detection were performed with the system on a real-time basis considering the following factors:

- Corners at different locations on the print bed
- Camera placed at different angles
- Different geometries of the corner

The test started with rectangular coupons with a length of 80 mm, a width of 8 mm and a height of 3 mm. The printer's parameters are listed in Table 2. In the beginning, the camera was perpendicular to the X-axis (orientation A). The rectangular coupon was printed at different locations on the print bed: up-left, center and down-right. Two trials were executed at each location, yielding a total of six coupons. Then, the camera was placed at 75 degrees above the X-axis (orientation B), facing at the center of the print area. Six coupons were printed at 3 different locations, again. Finally, the camera was brought back to 90 degrees to investigate the accuracy regarding different corner's geometries, which were rounded corners and sharp corners. Both geometries were coupons with a length of 80 mm, width of 8 mm and height of 3 mm. The rounded geometry had a circular corner with a radius of 4 mm. While, the sharp geometry had a triangular corner with a height of 15 mm. The results are shown in Table 3.

**Table 2. 3D printing parameters for the tests.**

| Manufacturing parameter | Value | Manufacturing parameter | Value |
|---|---|---|---|
| Print direction | XYZ | Nozzle diameter (mm) | 0.4 |
| Material | PLA | Nozzle temperature (°C) | 200 |
| Raster angle | 0 | Cooling | No fan cooling |
| Layer height (mm) | 0.15 | Infill (%) | 30 |
| Bed temperature (°C) | 60 | Filament diameter (mm) | 1.75 |
| Print speed (mm/min) | 2400 | | |

The coupon had a total number of 20 layers with a layer thickness of 0.15 mm. The system first allowed the print to be built up to about 1 mm. So, when the sixth layer was finished, the first picture was captured and analyzed. Based on the result, the OctoPrint plugins would stop the print (result < 0.3) or continue the print (result ≥ 0.3). Taking the test with a coupon at up-left of the print bed and a camera angle of 75 degrees (Table 3 and Figure 22), The first 13 layers analyzed (layer #6 to #18) were recognized as corners without warpage because the results were greater than 0.3. The 19th layer had a result of 0.000324 so that the print was terminated as a warp was detected.

**Table 3. Warping detection results of up-left position and camera at 75 degrees from layer #6 to #19.**

| Layer # | P (x = unwarped corner) | Layer # | P (x = unwarped corner) |
|---|---|---|---|
| 6 | 0.689 | 13 | 0.665 |
| 7 | 0.525 | 14 | 0.844 |
| 8 | 0.892 | 15 | 0.753 |
| 9 | 0.765 | 16 | 0.79 |
| 10 | 0.814 | 17 | 0.709 |
| 11 | 0.803 | 18 | 0.69 |
| 12 | 0.732 | 19 | 0.000324 |

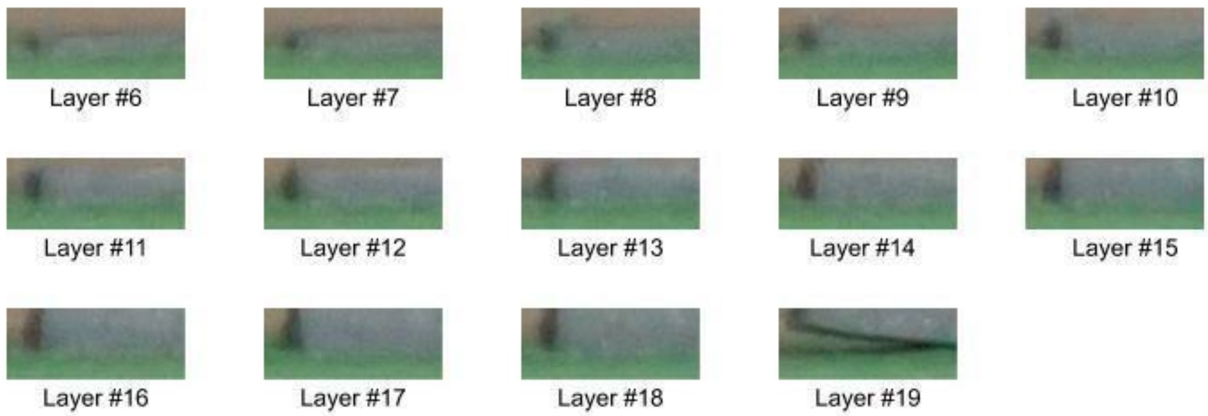


**Figure 22. Cropped images of up-left position and camera at 75 degrees from layer #6 to #19.**

Table 4 is the summary of the test results in terms of camera angles, coupon positions and different geometries. A total of 16 coupons were printed, and 128 images were captured, cropped and analyzed by the real-time in-process warping detection system. 127 images were correctly classified with an accuracy of 99.21%. Also, all the cropped images contained the coupon's corner, indicating the image cropping's precision of 100%. It can be observed that the system worked for both camera angles and all the three different positions with high accuracy. Further, this system can also identify the warping of rounded and sharp corners. The only image that was not correctly identified was from Test 8 in which the corner was warped since layer #6. The system did not recognize the warpage until layer #7. So, the print was terminated at layer #7 instead of layer #6.

It can be seen from Figure 22 that the cropped images of corners were blurry. This was because the upgraded system captured the corner's image right at where it stopped instead of delivering the coupon to a pre-determined location that is close to the camera, making an optimized focus distance unachievable. Nonetheless, high accuracy was acquired from the system despite the blurriness. Compared with the original CNN classification model, which took an image size of 525×100 pixels, the new model developed by Aditya Saluja could analyze images with a smaller size (100×40 pixels). Although the newer model was shallower, only 8 layers, as opposed to 21, proposed earlier, it had a higher number of feature maps in each layer. Having multiple feature maps allows the model to learn various features improving the performance of the model. In addition, by down-sampling the input image feature maps are invariant to shift, and distortion as seen by the results.

**Table 4. Test result summary.**

| Camera angle | Coupon position | Test number | Total number of analyzed layers | Number of unwarped layers | Number of warped layers | Layers correctly classified | Corners correctly cropped |
|---|---|---|---|---|---|---|---|
| 90 degrees | Downright | 1 | 11 | 10 | 1 | 11 | 11 |
| | | 2 | 9 | 8 | 1 | 9 | 9 |
| | Center | 3 | 10 | 9 | 1 | 10 | 10 |
| | | 4 | 3 | 2 | 1 | 3 | 3 |
| | Up-left | 5 | 13 | 13 | 0 | 13 | 13 |
| | | 6 | 5 | 4 | 1 | 5 | 5 |
| | Triangular corner | 7 | 14 | 14 | 0 | 14 | 14 |
| | | 8 | 2 | 0 | 2 | 1 | 2 |
| | Rounded corner | 9 | 11 | 10 | 1 | 11 | 11 |
| | | 10 | 4 | 3 | 1 | 4 | 4 |
| 75 degrees | Downright | 11 | 5 | 4 | 1 | 5 | 5 |
| | | 12 | 8 | 7 | 1 | 8 | 8 |
| | Center | 13 | 6 | 5 | 1 | 6 | 6 |
| | | 14 | 5 | 4 | 1 | 5 | 5 |
| | Up-left | 15 | 14 | 13 | 1 | 14 | 14 |
| | | 16 | 7 | 6 | 1 | 7 | 7 |

The assumption made at the beginning that the $y_{image}$ can be regarded as a constant was valid as the corners were precisely cropped for all images with a constant value assigned to $y_{image}$. If the camera is deployed with a high or low angle shot where $y_{image}$ cannot be treated as a constant, the same correlation methodology can be used to estimate its value. Moreover, this technique is not restricted to 3D printing. CNC machining is another field where the feature extraction system can be used to crop out the important regions of an image as the operations of CNC machines are also guided by G-code.

# 5. Conclusion

This report demonstrated a closed-loop in-process warping monitoring system on FFF 3D printing that coordinated and controlled the printer, camera, and a microcomputer. As a result, the upgraded warping detection model had an enhanced accuracy of 99.21%. Also, the image cropping functionality has been created to autonomously locate and crop out the corner from the original image, which mitigated the environmental noises and improved the accuracy. An automated correlation process was designed to perform map-matching between the print bed and the image coordinate systems to aid in feature extraction with high precision. Finally, the OctoPrint plugins served as the interfaced between the software and hardware, performing real-time G-code analysis and information transmission. The refined warping monitoring system exhibited high precision and accuracy with minimal error and no false positive.

Based on the results, the feature extraction methodology can be flexibly applied to a system with different camera angles. Thus, the system could potentially deploy cameras around the print bed to inspect more types of defects. Moreover, this technique is not restricted to 3D printing. CNC machining is another field where the feature extraction system can be used to crop out the important regions of an image as the operations of CNC machines are also guided by G-code.

## 6. References


1. S. Ford and M. Despeisse, “Additive manufacturing and sustainability: an exploratory study of the advantages and challenges,” *Journal of Cleaner Production*, vol. 137, pp. 1573–1587, 2016.

2. M. S. Alsoufi, M. W. Alhazmi, D. K. Suker, W. K. Hafiz, S. S. Almalki, and R. O. Malibari, “Influence of Multi-Level Printing Process Parameters on 3D Printed Parts in Fused Deposition Molding of Poly(lactic) Acid Plus: A Comprehensive Investigation,” *American Journal of Mechanical Engineering*, vol. 7, no. 2, pp. 87–106, 2019.

3. D. Dimitrov, W. V. Wijck, K. Schreve, and N. D. Beer, “Investigating the achievable accuracy of three dimensional printing,” *Rapid Prototyping Journal*, vol. 12, no. 1, pp. 42–52, 2006.

4. T. M. G. Muenchen, “Learning Course: Deep Dive Additive Manufacturing - Deep Dive: Additive Fertigung,” *Technology MAnagement Group*. [Online]. Available: https://www.tmg-muenchen.de/training-course/11/Additive-Manufacturing?flang=en. [Accessed: 01-Apr-2020].
5. I. Gibson, B. Stucker, and D. W. Rosen, *Additive manufacturing technologies: rapid prototyping to direct digital manufacturing*. New York: Springer, 2010.

6. Hodder, Kevin J., et al. “Process Limitations of 3D Printing Model Rock.” *Progress in Additive Manufacturing*, vol. 3, no. 3, 2018, pp. 173–182., doi:10.1007/s40964-018-0042-6.
7. Z. Chen, Z. Shen, J. Guo, J. Gao, and X. Zeng, “Line drawing for 3D printing,” *Computers & Graphics*, 02-Jun-2017. [Online]. Available: https://www.sciencedirect.com/science/article/pii/S0097849317300687. [Accessed: 14-Sep-2019].

8. B. N. Panda, K. Shankhwar, A. Garg, and Z. Jian, “Performance evaluation of warping characteristic of fused deposition modelling process,” *The International Journal of Advanced Manufacturing Technology*, vol. 88, no. 5-8, pp. 1799–1811, May 2016.

9. W. Gao, Y. Zhang, D. Ramanujan, K. Ramani, Y. Chen, C. B. William, C. Y. Wang, Y. C. Shin, S. Zhang, and P. D. Zavattieri, “The status, challenges, and future of additive manufacturing in engineering,” *Computer Aided Design*, pp. 65–89, 2015.
10. Liu, X. and V. Shapiro, *Homogenization of material properties in additively manufactured structures.* Computer-Aided Design, 2016. **78**: p. 71 82.
11. R. T. L. Ferreira, I. C. Amatte, T. A. Dutra, and D. Bürger, “Experimental characterization and micrography of 3D printed PLA and PLA reinforced with short carbon fibers,” *Composites Part B: Engineering*, vol. 124, pp. 88–100, 2017.

12. Cignoni, Paolo. *Schematic Representation of Fused Filament Fabrication*. 2017, commons.wikimedia.org/wiki/File:Schematic_representation_of_Fused_Filament_Fabrication_01.png.
13. Bitonti, Francis. *3D Printing Design: Additive Manufacturing and the Materials Revolution*. Bloomsbury Visual Art, 2019.
14. Seepersad, Carolyn Conner. “Challenges and Opportunities in Design for Additive Manufacturing.” *3D Printing and Additive Manufacturing*, vol. 1, no. 1, 2014, pp. 10–13., doi:10.1089/3dp.2013.0006.
15. Viotti, Matias R., and Armando Albertazzi. *Robust Speckle Metrology: Techniques for Stress Analysis and NDT*. SPIE Press, 2014.

16. Q. Y. Lu and C. H. Wong, “Additive manufacturing process monitoring and control by non-destructive testing techniques: challenges and in-process monitoring,” *Virtual and Physical Prototyping*, vol. 13, no. 2, pp. 39–48, 2017.

17. R. T. L. Ferreira, I. C. Amatte, T. A. Dutra, and D. Bürger, “Experimental characterization and micrography of 3D printed PLA and PLA reinforced with short carbon fibers,” *Composites Part B: Engineering*, vol. 124, pp. 88–100, 2017.

18. T.-M. Wang, J.-T. Xi, and Y. Jin, “A model research for prototype warp deformation in the FDM process,” *The International Journal of Advanced Manufacturing Technology*, vol. 33, no. 11-12, pp. 1087–1096, 2006.

19. A. Armillotta, “Assessment of surface quality on textured FDM prototypes,” *Rapid Prototyping Journal*, vol. 12, no. 1, pp. 35–41, 2006.

20. Tyson, Ed. “3D Prints Warping or Curling? – Why It Happens and How to Prevent It.” *Rigid.ink*, 2015, rigid.ink/blogs/news/3d-prints-warping-why-it-happens-and-how-to-prevent-it.

21. E. R. Fitzharris, N. Watanabe, D. W. Rosen, and M. L. Shofner, “Effects of material properties on warpage in fused deposition modeling parts,” *The International Journal of Advanced Manufacturing Technology*, vol. 95, no. 5-8, pp. 2059–2070, 2017.

22. A. Peng and X. Xiao, “Investigation on Reasons Inducing Error and Measures Improving Accuracy in Fused Deposition Modeling,” *INTERNATIONAL JOURNAL ON Advances in Information Sciences and Service Sciences*, vol. 4, no. 5, pp. 149–157, 2012.

23. M. S. Alsoufi and A. E. Elsayed, “Warping Deformation of Desktop 3D Printed Parts Manufactured by Open Source Fused Deposition Modeling (FDM) System,” *International Journal of Mechanical & Mechatronics Engineering*, 2016.

24. K. Singh, “Experimental study to prevent the warping of 3D models in fused deposition modeling,” *International Journal of Plastics Technology*, vol. 22, no. 1, pp. 177–184, 2018.

25. A. Armillotta, M. Bellotti, and M. Cavallaro, “Warpage of FDM parts: Experimental tests and analytic model,” *Robotics and Computer-Integrated Manufacturing*, vol. 50, pp. 140–152, 2018.

26. A. Guerrero-De-Mier, M. Espinosa, and M. Domínguez, “Bricking: A New Slicing Method to Reduce Warping,” *Procedia Engineering*, vol. 132, pp. 126–131, 2015.

27. Milovanović, Bojan, and Ivana Banjad Pečur. “Review of Active IR Thermography for Detection and Characterization of Defects in Reinforced Concrete.” *Journal of Imaging*, vol. 2, no. 2, 2016, p. 11., doi:10.3390/jimaging2020011.

28. Lu, Yanglong, and Yan Wang. “Monitoring Temperature in Additive Manufacturing with Physics-Based Compressive Sensing.” *Journal of Manufacturing Systems*, vol. 48, 2018, pp. 60–70., doi:10.1016/j.jmsy.2018.05.010.

29. Li, Yongxiang, et al. “In-Situ Monitoring and Diagnosing for Fused Filament Fabrication Process Based on Vibration Sensors.” *Sensors*, vol. 19, no. 11, 2019, p. 2589., doi:10.3390/s19112589.

30. Wu, Haixi, et al. “In Situ Monitoring of FDM Machine Condition via Acoustic Emission.” *The International Journal of Advanced Manufacturing Technology*, 2015, doi:10.1007/s00170-015-7809-4.

31. Wu, Haixi, et al. “Real-Time FDM Machine Condition Monitoring and Diagnosis Based on Acoustic Emission and Hidden Semi-Markov Model.” *The International Journal of Advanced Manufacturing Technology*, vol. 90, no. 5-8, 2016, pp. 2027–2036., doi:10.1007/s00170-016-9548-6.
32. Fang, Liang, et al. “Application of Embedded Fiber Bragg Grating (FBG) Sensors in Monitoring Health to 3D Printing Structures.” *IEEE Sensors Journal*, vol. 16, no. 17, 2016, pp. 6604–6610., doi:10.1109/jsen.2016.2584141.
33. Kousiatza, Charoula, and Dimitris Karalekas. “In-Situ Monitoring of Strain and Temperature Distributions during Fused Deposition Modeling Process.” *Materials & Design*, vol. 97, 2016, pp. 400–406., doi:10.1016/j.matdes.2016.02.099.
34. J. Straub, “Initial Work on the Characterization of Additive Manufacturing (3D Printing) Using Software Image Analysis,” Machines, vol. 3, no. 2, pp. 55–71, 2015.
35. F. Baumann and D. Roller, “Vision based error detection for 3D printing processes,” MATEC Web of Conferences, vol. 59, p. 06003, 2016.
36. O. Holzmond and X. Li, “In situ real time defect detection of 3D printed parts,” Additive Manufacturing, vol. 17, pp. 135–142, 2017.
37. C. Liu, A. C. C. Law, D. Roberson, and Z. Kong, “Image analysis-based closed loop quality control for additive manufacturing with fused filament fabrication,” Journal of Manufacturing Systems, vol. 51, pp. 75–86, 2019.